JACS
JOURNAL OF THE AMERICAN CHEMICAL SOCIETY

Article

pubs.acs.org/JACS

ILQINS Hexapeptide, Identified in Lysozyme Left-Handed Helical Ribbons and Nanotubes, Forms Right-Handed Helical Ribbons and Crystals

Cecile Lara,[†] Nicholas P. Reynolds,[‡] Joshua T. Berryman,[§] Anqiu Xu,[±] Afang Zhang,[±] and Raffaele Mezzenga*[,†]

[†]Food & Soft Materials, Department of Health Science & Technology, ETH Zurich, Schmelzbergstrasse 9, LFO, E23, 8092 Zürich, Switzerland

[‡]Materials Science and Engineering, CSIRO, Private Bag 10, Bayview Avenue, Clayton, Vic 3169, Australia

[§]Faculty of Science Technology and Communication, University of Luxembourg, 162a Avenue de la Faïencerie, L-1511 Luxembourg

[±]Department of Polymer Materials, Shanghai University, Nanchen Street 333, Shanghai 200444, China

Supporting Information

ABSTRACT: Amyloid fibrils are implicated in over 20 neurodegenerative diseases. The mechanisms of fibril structuring and formation are not only of medical and biological importance but are also relevant for material science and nanotechnologies due to the unique structural and physical properties of amyloids. We previously found that hen egg white lysozyme, homologous to the disease-related human lysozyme, can form left-handed giant ribbons, closing into nanotubes. By using matrix-assisted laser desorption ionization mass spectrometry analysis, we here identify a key component of such structures: the ILQINS hexapeptide. By combining atomic force microscopy and circular dichorism, we find that this fragment, synthesized by solid-phase peptide synthesis, also forms fibrillar structures in water at pH 2. However, all fibrillar structures formed possess an unexpected right-handed twist, a rare chirality within the corpus of amyloid experimental observations. We confirm by small- and wide-angle X-ray scattering and molecular dynamics simulations that these fibrils are composed of conventional left-handed β-sheets, but that packing stresses between adjacent sheets create this twist of unusual handedness. We also show that the right-handed fibrils represent a metastable state toward β-sheet-based microcrystals formation.

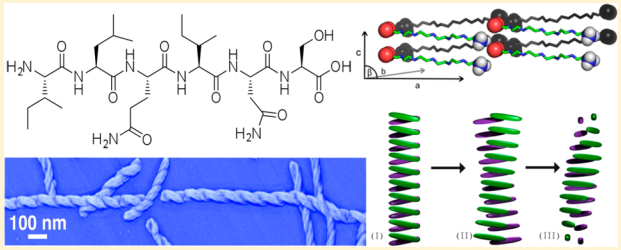

INTRODUCTION

Amyloid fibrils are extensively studied as disease-related assemblies, since they are involved in several neurodegenerative pathologies.[1,2] However, it has been suggested that mature amyloid fibrils are nontoxic byproducts of disease and that neurotoxicity arises from either prefibrillar aggregates,[3−5] or the assembly process itself,[6−8] and some fibrils have been shown to bear functional activity.[9−11] Amyloids moreover have interesting mechanical properties[12,13] and are thus advantageous as nontoxic bionanomaterials for applications in various fields, ranging from biomaterials[14,15] to electronics.[16,17] Fibrils are generally <100 nm in diameter, several micrometers long, and can assemble together to form multistranded aggregates. They share a β-sheet rich structure organized in a cross-β pattern.[18,19] Considerable work is thus focused on understanding the mechanisms of self-assembly and on characterizing the fibrillar structures obtained. Numerous proteins have been demonstrated to undergo amyloid-like self-assembly in vitro, suggesting a general ability of proteins to form fibrils, provided the proper conditions are identified.[20,21] A large diversity in fibril structures does nevertheless exist, since different β-sheet arrangements can occur[22] with variable side chains interactions and steric-zipper motifs.[23−25] Several synthetic peptides have also been shown to assemble into fibrillar structures, with varying morphologies, including nanotubes, flat sheets, helical ribbons, and crystals.[26−28] Hen egg white lysozyme (HEWL) is known to form fibrils at high temperature and acidic conditions.[29,30] Indeed, all structured proteins are thought to contain aggregation-prone regions, buried in their hydrophobic core.[31] Several peptide fragments in the HEWL sequence were found to be involved in amyloid formation, whether obtained by proteolysis or hydrolysis.[30,32] In our previous works, we observed the formation of giant multistranded lateral assemblies of left-handed HEWL fibrils, driven by hydrolysis of the native protein,[33] and their eventual closure into nanotubes.[34] We here identify, by matrix-assisted laser desorption ionization mass spectrometry (MALDI-MS), the most significant constitutive fragments of those fibrillar structures, all of which contain the ILQINS hexapeptide. The self-assembly of the synthesized

Received: January 23, 2014
Published: March 3, 2014

   dx.doi.org/10.1021/ja500445z | J. Am. Chem. Soc. 2014, 136, 4732−4739

peptide was experimentally investigated in order to determine the morphology of the aggregation products while following the assembly process. Atomic force microscopy (AFM) was used as the main tool to image the formation of rarely observed right-twisted helical ribbons and their conversion to microcrystals. Additional evidence for this ribbon-to-microcrystal conversion was provided by small angle-X-ray scattering experiments (SAXS). Single molecule statistical analysis of the images further provided information about the fibrils flexibility and crystals dimensions. Molecular dynamics (MD) simulations of the ILQINS aggregates were used to generate atomistic structures consistent with the results from AFM, circular dichroism (CD), and wide-angle X-ray scattering (WAXS) experiments. The simulations also provided a compelling structural explanation for the unusual right-twisted morphology observed. Taken together, these results offer an atomistic rationale for the establishment of the handedness of the ILQINS hexapeptide aggregates and can serve as a basis to the understanding of the factors which play a role in defining the macroscopic chirality of amyloid-like fibrous aggregates from proteins and peptides.

RESULTS AND DISCUSSION

MALDI-MS Reveals a Common Aggregating Sequence From HEWL. The HEWL amyloid multistranded ribbons and nanotubes are composed of short fragments generated during hydrolysis of the native protein.[33] In Figure 1,

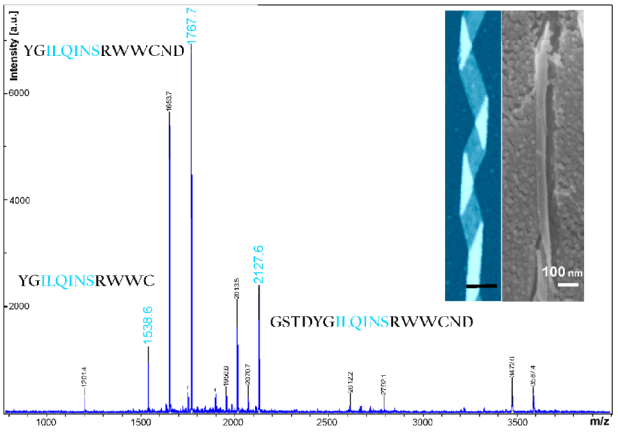

Figure 1. MALDI-MS spectra of the HEWL helical ribbons and nanotubes, AFM height image, and SEM picture insets, with scale bars 100 nm. The most probable amino acid sequences, corresponding to the peaks marked in blue, are inserted in the figure.

the MALDI-MS spectrum shows different peaks corresponding to mass over charge ratios (m/z) below 4000 Da. Interestingly, most of the matching sequences, identified in the spectrum analysis report (Figure S1), contain the ILQINS fragment. Three examples of sequences, corresponding to the masses highlighted in blue, are given in Figure 1. These results are in line with the findings of Krebs et al.,[34] who demonstrated that the residues 49−64 (GSTDYGILQINSRWWC), coming from the β-sheet region of native HEWL, show a tendency to aggregate into fibrils.[34] However, the much larger fragment 57−107 (QINS...ALL...MNA) was also shown to form fibrils at pH 2, and 37 °C.[30] It becomes then highly desirable to understand whether smaller sequences among those reported above are sufficient to induce fibrillization.

To our knowledge, no evidence of ILQINS fibrillization in water has been previously observed, and although several works on synthetic peptides consider the ILQINS (hexapeptide 55−60) as a fibril-forming fragment,[23,35] they all rely on the experimental evidence of the larger 49−64 synthetic peptide as a fibril forming constitutive block.[34] In what follows we investigate whether the 55−60 fragment is sufficient to induce aggregation on its own, as can be predicted by comparing the outcome from three different algorithms[31,35] designed to predict fibril-forming regions from protein sequences (for the predictions using the different methods see Figure S2). In particular, we intend to determine if this hexapeptide is the primary building block responsible for promoting the fibrillization and lateral assembly mechanism previously observed for native HEWL.[33,36] We thus chose to focus here on the fibrillization of the ILQINS hexapeptide and compare it to previously observed fibril formation from HEWL.[33,36] The ILQINS sequence (Scheme S1) was synthesized by standard solid-phase peptide synthesis. The hexapeptide was characterized by proton NMR spectroscopy (Figure S3) and MS (Figure S4).

ILQINS Forms Metastable Right-Handed Helical Ribbons at Room Temperature, Which Are Converted to Microcrystals at Longer Incubation Times. In order to compare the ILQINS self-assembly to the HEWL fibrillization, similar experimental conditions are used. Surprisingly, when dispersed in pH 2 Milli-Q water at 90 °C and at 1 mg/mL concentration upon stirring, the ILQINS powder dissolves completely and does not lead to any obvious self-assembly (no fibrils found by AFM, negligible changes in CD ellipticity, and UV absorption in the 200−250 nm range after 18 h, see Figure S5).

In view of the control low-temperature experiments to be discussed extensively below, these puzzling results remain to be elucidated in full, although they suggest that while at 90 °C ILQINS is present as a molecular solution, at room temperature aggregation of ILQINS proceeds via a seeded fibrillation kinetics, where the presence of unmelt preaggregates can act as seeds. It has indeed been shown previously that the critical aggregation concentration for fibrillization-prone oligopeptides, (settling the threshold for the presence of seeds) tends to vanish with increasing temperatures.[37] By any events, high temperature is clearly not promoting the self-assembly of the ILQINS fragment, possibly even preventing aggregation. This confirms our previous findings that the role of the 90 °C treatment at pH 2 is primarily to promote native HEWL unfolding and hydrolysis into shorter segments.[33]

In sharp contrast, by dispersing via gentle stirring ILQINS (1 mg/mL) in Milli-Q water (pH 2) at room temperature, aggregation does occur. When imaged 5 min after mixing, the sample already contains long fibrils and fibrillar aggregates (Figure S6). Multistranded helical ribbon structures are seen in the AFM images at incubation times up to 1.5 h, as shown in Figure 2a.

Interestingly, all ribbons show a right-handed twist as depicted in Figure 2b, which contrasts with the case of native HEWL incubation, where left-handed ribbons are solely formed. A surprising study showed that the directionality of vortex motion was sufficient to induce chiral symmetry breaking in aggregates of porphyrin molecules due to hydrodynamic and steric effects generated during aggregation.[38] Thus, it should be mentioned at this stage that control experiments were run to demonstrate that both clockwise and

dx.doi.org/10.1021/ja500445z | J. Am. Chem. Soc. 2014, 136, 4732−4739

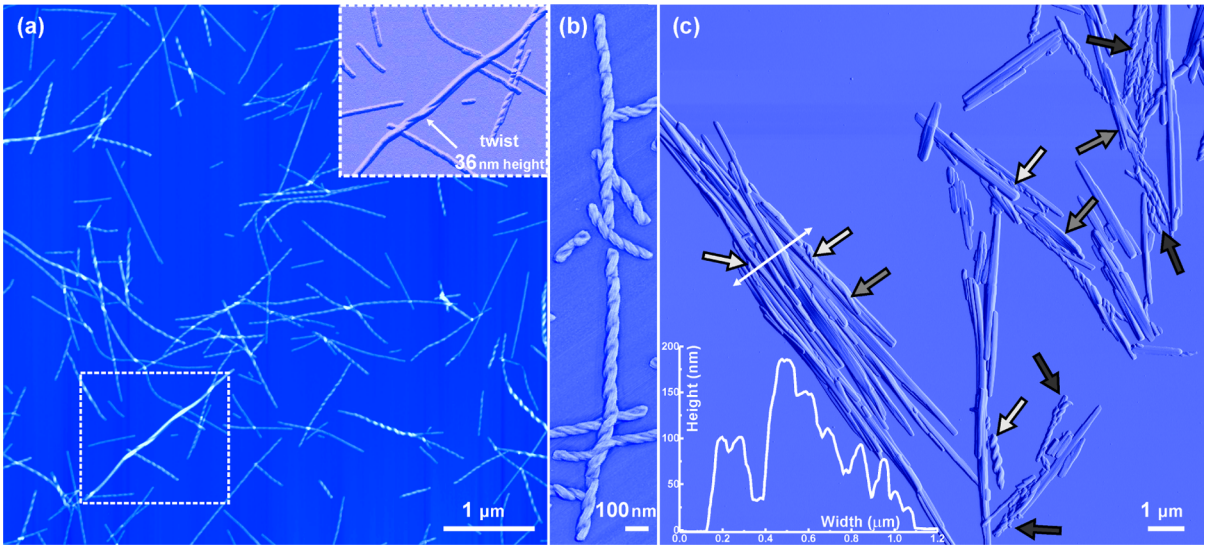

Figure 2. (a) AFM height image of ILQINS helical ribbons after 1.5 h stirring, inset zoom amplitude image of a thicker partially twisting ribbon. (b) Phase image of right-handed helical ribbons. (c) Amplitude image of the crystals formed after 24 h incubation. White arrows show helical ribbons, gray arrows twisting crystal sheets, and black arrows lateral assembly of ribbons. The plot shows the AFM height profile along the white arrow.

counter-clockwise stirring always lead to right-handed structures for ILQINS. The understanding of the factors defining macroscopic chirality in amyloid fibrils is still in its infancy,[39] and occurrence of right-handedness contrasts sharply with the general assumption that (*S*)-amino acids usually form left-handed fibrils.[40,41] Evidence of right-handed fibrils from natural (*S*)-amino acid sequences, or handedness inversion during either pH changes or fibrillization progressing, has indeed been shown only in rare cases.[42−45] The phenomenon of right-handed twists so far lacks an explanation in terms of atomistic structure. Formation of unspecified non-β structure has been mooted as a cause[42] and also evidence from mutation studies points to the importance of terminus residues, in turn suggesting tertiary assembly across β-sheet edges as the root of the phenomenon.[40] Although morphological evidence of right-twisted fibrils is rare, vibrational CD studies have also indicated mirror image patterns of ellipticity in insulin fibrils of zero overall twist,[43] which suggests that this and perhaps some of the other untwisted aggregates which are commonly observed may contain a balance of right- and left-twisted substructures. Finally, inversion of chirality (from left-handed to right-handed) during fibrillization of serum albumin has recently been shown to occur as a result of increasing polymorphism complexity during fibril self-assembly.[39,44]

In the present case, the observed change in handedness between the HEWL and ILQINS fibrils suggests that the structure of the HEWL giant ribbons and nanotubes[33,34] is not only based on the ILQINS self-assembly but also is strongly dependent on the additional amino acids present in the sequences identified, which could alter the fibril core structure or could simply govern the arrangement in a different manner through side-chain interactions. The presence of several peaks in Figure 1 also suggests a composite assembly made of different fragments in the case of HEWL fibrils. Indeed, different from the fibrillization process with chirality inversion,[44] in the present case right-handedness is maintained throughout the entire process, until a new needle-like crystal morphology starts to emerge after several hours incubation at room temperature (Figure 2c). A precursor of the needle-like crystals is depicted in the inset image in Figure 2a, where a thicker fibrillar aggregate with a loose twisting without regular periodicity is shown. Such structures are thought to be unfolding intermediates, built from the lateral assembly of helical ribbons. Partial unfolding of the helical ribbons to form flatter sheets, as suggested for crystallization of cholesterol,[46] eventually stacking on top of each other, could explain the morphology observed with increasing incubation time, as shown in Figures 2c and S6. The inset height profile in Figure 2c demonstrates that several layers are piled up, with heights reaching 200 nm, more than 15-fold the height of the initial helical ribbons. Some crystals are even thicker (Figure S7).

Such a fibril-to-crystal transition was observed previously for synthetic peptides such as GNNQQNY and NNQQNY from the prion protein, with crystal and fibrillar structure being strongly correlated.[18,19,47,48] Our findings also show that aromatic interaction cannot be considered here as the driving force for fibril-to-crystal transition as previously suggested,[44,46] but that shear forces from stirring can help faster crystalline arrangement as observed for GNNQQNY in a Couette cell.[47] Several further peptides were shown to form fibrils and also to crystallize.[23,47−50] The conditions used to promote crystal growth however usually differ from those used to induce fibrillation (standard crystal growth methods use vapor diffusion hanging drop setup, using additives to promote precipitation and crystallization).[23,25] Here we show a direct fibril to crystal switch, in the same experimental conditions, as previously reported for the GNNQQNY peptide.[45] In Figure 3a, the AFM height image shows a right-handed ribbon formed after 1.5 h stirring at room temperature. The white arrow points to the splitting right end, showing that the ribbon is made of two intertwined filaments. It thus corresponds to a not yet totally folded profile, with variation in height and half-pitch (distance between two consecutive maxima) along the contour length, as shown in Figure 3b. Only the height of the perfectly folded left-side extremity corresponds to the most frequent height, as shown in the height distribution profile in Figure 3c. Most of the ribbons are around 13 nm high, and the pitch varies between 40 and 90 nm, depending on the folding and on the height (number of protofilaments) as shown in Figure 2a. The average persistence length L_p of those fibrils, determined

dx.doi.org/10.1021/ja500445z | J. Am. Chem. Soc. 2014, 136, 4732−4739

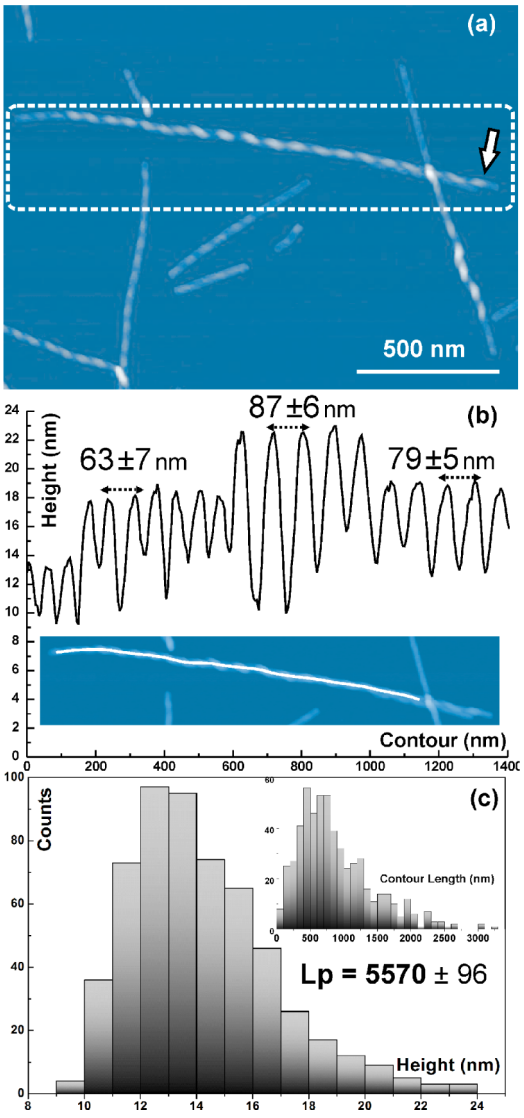

Figure 3. (a) AFM height image of a helical ribbon, splitting in two ribbons at its right end (white arrow), and (b) with variable height and pitch along its contour length. c) Height distribution of the helical ribbons formed after 1.5 h stirring at room temperature and corresponding contour length distribution.

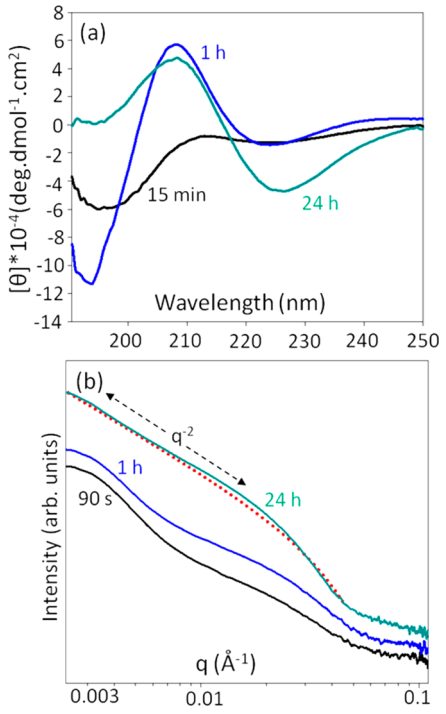

Figure 4. (a) CD spectra of the ILQINS hexapeptide in pH 2 water in molecular ellipticity at three different times during the incubation process. Prior to each measurement solution was diluted to 0.33 mg/mL. (b) SAXS spectra at 90 s and 1 and 24 h, (0.0025−0.15 $Å^{-1}$) together with the fit generated from the form factor of an infinitely large flat homogeneous particle of thickness 9.8 nm (red dashed line). For the 24 h SAXS spectra in the very low q regions show a q^{-2} dependence indicative of a flat 2D particle due to microcrystal formation.

by fitting with the bond correlation function, $\langle \cos\theta(s) \rangle \approx e^{-(s/2Lp)}$, where θ is the angle between the tangent vectors to the chain at two points separated by a contour distance (s), extracted from the statistical analysis of the AFM images,[49] is ~5 μm, indicating a very rigid structure.

In Figure 4a, the CD measurements depict the secondary structure evolution with incubation time. The mainly random structure, 15 min after mixing, identified by a minimum below 200 nm and weak ellipticity above this wavelength, can be explained by an only partial conversion of the hexapeptide into helical ribbons at this early stage. After 1 h, when mainly helical ribbons are present in solution, a strong ellipticity is observed, indicating the formation of β-structure, consistent with the signal observed for the 59−81 fragment or the 41−60 residues assemblies from HEWL, with maximum at 205 nm and minimum in the 225−230 nm region.[50,51] This signal is associated with strongly twisted β-sheets[52] and will be supported by WAXS crystal analysis and MD simulations, as shown later in this manuscript. The profile recorded at 24 h also shows a clear maximum at 205 nm and a broad minimum between 225 and 230 nm indicating the continued presence of β-sheets from the stacking of the ILQINS peptide, even though the helical ribbons are almost fully converted into needle-like crystals at this stage.

Small-Angle X-ray Scattering Provides Further Evidence for Rapid Aggregation and the Development of Microcrystals. SAXS spectra from a synchrotron source were recorded at scattering vectors in the range of 0.0025−0.15 $Å^{-1}$ (Figure 4b). From these spectra we can gain some information on the overall morphology of the fibrils and also investigate deeper the observed ribbon-crystal conversion. The initial spectra recorded in the first 10−15 min of the process clearly possess a Guinier region at low scattering vectors (in the region of ~0.002−0.006 $Å^{-1}$). Guinier analysis[53] revealed a radius of gyration (R_g) of 54.1 nm. Assuming a thin rod-like morphology where the contour length (L) is much larger than the cross-section of the rod $R_g^2 = (1/12)L^2$.[54] Thus, we can calculate a mean contour length (L) of 187.4 nm for the protofilaments that are generated at very early time points (90 s). As the aggregation time increases, the contour length increases beyond the maximum observable window available to the SAXS detector, thus the Guinier region is lost after around 15 min, at which time the mean contour length is calculated to be 193.4 nm. By comparing this value to the contour lengths calculated by statistical analysis of the AFM data taken after 90 min (inset in Figure 3c) one notes that there is a high population of filaments with a contour length ranging between 500 and 1000 nm. The rapid increase in contour length to almost 200 nm

dx.doi.org/10.1021/ja500445z | J. Am. Chem. Soc. 2014, 136, 4732−4739

after 15 min suggests that the ILQINS peptide nucleates very quickly, producing relatively short aggregates or protofibrils. For a wide variety of proteins amyloid aggregation is often proceeded by a lag phase (up to 5 h), allowing small oligomers to be nucleated (in a series of thermodynamically unfavorable steps) which are able to seed amyloid growth.[53] However, it should be noted that there are some examples of functional amyloids that can form with no observable lag phase.[1] The reasons for this rapid nucleation of the hexapeptide into micrometer-scale fibrils are currently uncertain. Possible explanations for this lack of observable lag phase may include a partition of the dispersed ILQINS peptides to the water−air interface, resulting in accelerated nucleation in the presence of a hydrophobic interface,[55,56] constantly renewed by stirring. Alternatively, and most probably, aggregation could be promoted via seeding from hexapeptide preaggregates from the added ILQINS powder, which is also strongly supported by the control experiments run at 90 °C. Finally, the rapid aggregation may also be inherent to the amyloidogenic nature of the ILQINS fragment (inferred from its presence in all MALDI-MS fragments observed in Figure 1). Based on the above, we propose that ILQINS contains only the primary sequence required for fibril formation and no extraneous secondary sequences.

The initial aggregation steps may be much faster compared to larger fibrillating proteins containing both amyloidogenic and nonamyloidogenic sequences. The large increase in contour length between 15 min (193.4 nm) and 90 min (500−1000 nm) is typical of fibrils growing in an exponential amyloid growth phase.[57] Looking now at the spectrum recorded at 24 h (Figure 4b), we can see that at low scattering vectors (q) the slope of the spectrum has a characteristic q^{-2} dependence, indicative of a flat 2D particle.[53] This development of the q^{-2} slope at longer time periods provides further experimental evidence for the fibril-crystal conversion seen in the AFM images recorded after longer reaction times (Figure 2c). Accordingly, the spectra at 24 h can be fitted almost perfectly (R^2 = 0.998) to the form factor of infinitely large, homogeneous flat particles of thickness (D) 9.8 nm, displayed as a red dotted line in Figure 4b (see Figure S8 for details of curve fit).

Wide-Angle X-ray Scattering Shows Unit Cell Parameters That Can Be Used As the Basis for the Simulation of an Atomic Structure. WAXS spectra from a synchrotron source were recorded in the range 0.3−0.68 Å $^{-1}$ (Figure 5a) at regular intervals of time throughout the peptides assembly. At around 90 s after the aggregation was initialized, a faint peak could be seen at 0.64 Å $^{-1}$ (Figure 5a). This peak corresponds to a d-spacing of 0.97 nm and thus can be assigned to the intermolecular β-sheet stacking distance of the growing protofilaments.[17,23,58] The spectrum shows that the assembly of the peptide is rapid and supports the observation of many multifilamentous structures in the AFM images after only 1.5 h (Figure 2a). As the reaction progresses, a second peak at 0.32 Å $^{-1}$ (d-spacing = 2.0 nm) and two additional peaks at 0.4 Å $^{-1}$ (1.55 nm) and 0.48 Å $^{-1}$ (1.3 nm) begin to appear.

Using the peaks from the WAXS spectra as a guide, a hypothetical unit cell for the aggregated ILQINS structure was designed by hand, starting from the known crystal structure for the similar sequence NNQQNY.[23] The designed unit cell contained two peptides in a yin-yang shape, with the central Q residues of the ILQINS sequence forming a docked pair of glutamine ladders, as for NNQQNY. A nanocrystalline

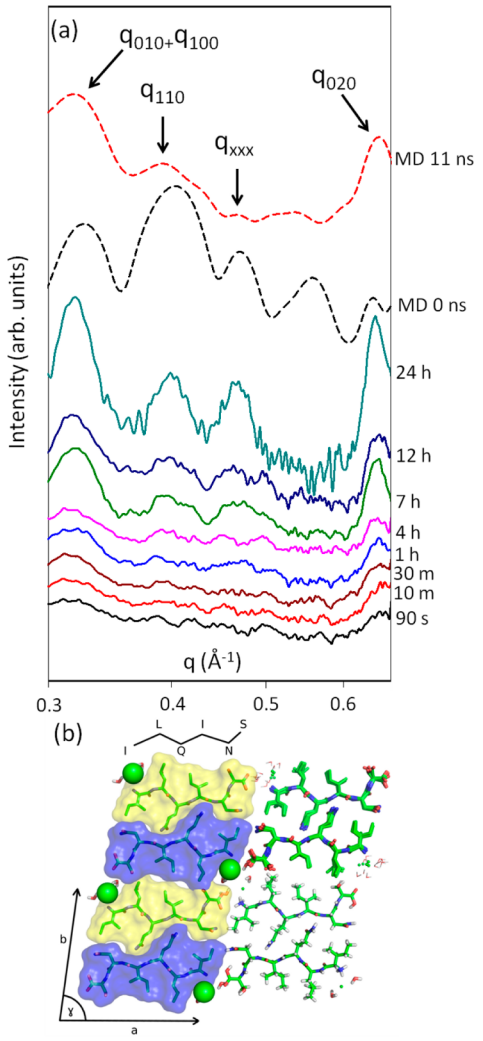

Figure 5. (a) Representative WAXS spectra (0.3−0.68 Å $^{-1}$) at various stages in the self-assembly of the ILQINS peptide from 90 s to 24 h; the dashed lines show calculated spectrum of the initial designed structure prior to MD (black), which underwent substantial conformational change, as shown in the calculated spectrum for the MD snapshot of the 1024-peptide nanocrystal taken at 11 ns (red). Labels show peaks to which it was possible to assign specific Miller indices, excepting q_{XXX} which appears to be a high-order reflection with multiple possible indexations. (b) A structure consistent with the X-ray data. Four unit cells are shown in the a−b plane. The left two cells show water and heavy atoms only, together with the solvent-exclusion surfaces of each peptide and chloride ion. The top-right cell shows the ensemble of cluster centers observed, in order to indicate labile regions of the structure. The lower-right cell shows all atoms of the peptides.

structure of 8 × 8 × 8 dimer unit cells (making a rhombic prism of approximately 16 × 12 × 3.5 nm) was then built by copying the two-peptide unit along lattice vectors of $a \approx b \approx 20$ Å (based on the peak assigned to $q_{010+}q_{100}$ in the X-ray spectrum) and, orthogonal to the a−b plane, c = 4.86 Å. The structure was allowed to relax in explicit water, containing 1024 chloride ions to neutralize the charges of the N-termini of the peptides, for 11 ns. During the first 5 ns, solvent molecules gradually entered the structure establishing disordered 'water columns' at the corners of the unit cell. The converged structure produced a spectrum qualitatively consistent with the X-ray data, suggesting that it is correct in its major features. The

dx.doi.org/10.1021/ja500445z | J. Am. Chem. Soc. 2014, 136, 4732−4739

peaks labeled $q_{010+}q_{100}$ and q_{110} result from Bragg reflections in the $a-b$ plane, and their assignment to the corresponding specific Miller indices is guided by an oblique columnar array symmetry.[59] The large peak q_{020} is straightforwardly assigned to the intermolecular β-sheet stacking distance manifested spontaneously over the course of the simulation (Figure 5b) and expected based on the typical fingerprint of amyloids.[17,23,58] The other expected amyloid peak q_{001}, corresponding to 4.6−4.8 Å, corresponding to the expected β-strand distance,[60] is out of the WAXS synchrotron range of Figure 5a but is correctly captured by the simulated structure in Figure 5b, although potentially other structures might also conform to the spectrum.

Examination of Atomic Structure. The structure generated has lattice vector lengths a = 21.7(±0.3)Å, b = 19.7(±0.3)Å, c = 4.9(±0.1) and angles α = 91(±3)°, β = 93(±4)°, and γ = 76(±3)° values in brackets are RMS fluctuations. The ensemble of calculated structures shown in the top-right cell of Figure 5b indicates that the central (Q_3) Glutamine zipper of ILQINS is extremely solid. The I_1 and L_2 residues rotate around the $C_\alpha-C_\beta$ bond quite freely but remain otherwise in place. The I_4 isoleucine stack is also very stable. The N_5 asparagine ladder undergoes minor fluctuations but with only transient interruption to its hydrogen bond ladder. The S6 side-chain and C-terminus are strongly coupled to the water column and are therefore very labile. The solvent-exclusion surfaces show that the steric packing of the system is tightest at the Q_3 zipper and also tight at the hydrophobic face, but looser around the water column.

Illustration of Stress Leading to Right-Twist. A view of the crystal structure in the $a-c$ plane illustrates the stress frozen into the crystal structure, which is relieved by twisting to the right (Figure 6). This diagram provides a structural mechanism for the unusual phenomenon of right-handed fibril twist and explains why it has been observed to be sensitive to mutations of the terminus residues.[40]

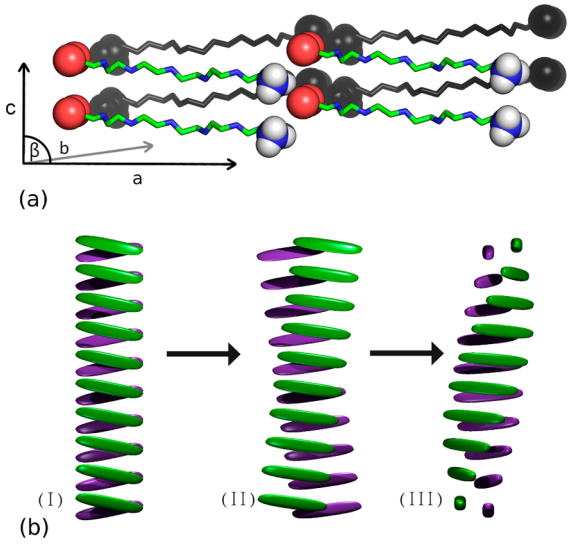

Figure 6. (a) Backbone structures of two unit cells shown in the $a-c$ plane. The strands furthest away are shown in gray. The strands are not perpendicular to the c-axis, which introduces a shear-stress between vertically adjacent peptides. (b) Diagram (I) illustrates two sheets of the stressed peptides. Part (II) shows a counterfactual structure, which would relax the shear stress, but introduce a mismatch at the buried IQN steric zipper. Part (III) introduces a right-handed twist, thus fixing the mismatch while retaining the angling of the sheets and the relaxation of the shear.

According to the proposed mechanism, there are two symmetry-breaking steps that take place: the first is the up−down symmetry of the peptide backbone. In the structures observed, the peptides are angled upward in the N−C direction, which introduces an elastic stress between vertically adjacent peptides (Figure 6b (I)). The second symmetry that must be broken is the choice of an axis of rotation for the fibril to twist about. For ILQINS, this is the Q_3 steric zipper. If one of the two symmetry breakings were to occur in the opposite sense (either backbone pointing down N−C, or I_4 stack at the center of rotation), then the phenomenon would serve only to reinforce the normal left-handed twist of the fibril. From Figure 5b and from the established strength and tightness of Q/N zipper motifs,[23,61] it is not surprising that the axis of rotation should be the IQN face of the peptide.

From Figure 6 it appears that the shearing of the peptide backbones out of the $a-b$ plane is driven by interdigitation of the double lone-pair bearing oxygen from the (protonated) C-terminus with the positively charged N-termini above and below. In order to be in contact with both the upper and lower terminus atoms of the adjacent sheet, the termini must necessarily be displaced up or down.

That the C and N termini point in different directions is already fixed by the even-numbered sequence length of the ILQINS chain (for odd numbered sequences, the C and N termini of a relaxed chain point off-axis in the same direction). That interdigitation of the termini leads to shearing of the sheets, rather than a simple mass displacement along the c-axis, is a more subtle issue. The requirement for this is probably what makes the right-twist so rare. In the case of this system it is possible that the attraction between N_5 residues of adjacent sheets contributes to preventing the β-sheets from interdigitating their termini simply by sliding past each other along the c-axis. A further consequence of the dependence of morphology on interdigitation of the termini is that right-twisted fibril growth therefore requires assembly to take place along the a-axis of the lattice; fibrils formed of the same monomer which assemble primarily along the b-axis will be left-twisted or rectangular, without any significant difference to the unit cell structure.

To test the hypothesis that (given the candidate peptide-dimer structure derived from simulation) the interdigitation of the termini is necessary to induce the abnormal right-handed twist, two simple simulations were run. One simulation was of two β-sheets of 16 ILQINS peptides joined by the usual IQN zipper, and one simulation was of four sheets: two copies of the two-sheet zipper system, with the termini adjacent. The two-sheet system was initialized with a right-handed twist and the four-sheet system with a left-handed twist. After a short MD simulation, each system rotated into the opposite twist to its starting configuration and remained in the new twisted conformation (Figure 7). This simple experiment shows that the terminus interactions along the a-axis of the crystal (the sterics and electrostatics of the N_5S_6 to I_1 packing) are required to induce the right-handed twist.

The SAXS and WAXS data combined with the associated MD simulations are in good agreement with the AFM results, thus confirming that the ILQINS fragment aggregates very rapidly into short right-handed helical ribbons fibrils whose contour length propagates in a typical amyloid exponential growth phase. Further incubation at pH 2 for a number of

dx.doi.org/10.1021/ja500445z | J. Am. Chem. Soc. 2014, 136, 4732−4739

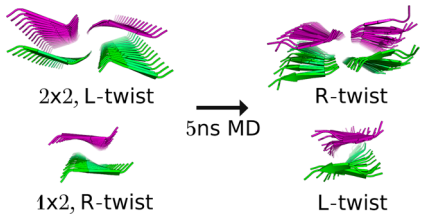

Figure 7. The importance of terminus interactions in the direction of the peptide axis is demonstrated by comparing a system in which axially adjacent sheet termini are present (2 × 2) to an identical one without axially adjacent sheets (1 × 2). Right-handed twisting is preferred only for the 2 × 2 system.

hours results in a conversion of the helical ribbons into flat crystalline structures. To the best of our knowledge this study discloses for the first time the structural self-assembly scheme and kinetics of ILQINS hexapeptide into coexisting amyloid-based helical ribbons and crystals formed under the same experimental conditions in water and provides a compelling molecular mechanism for the development of right-handed chirality in amyloid fibrils generated from short peptide sequences.

The explanation provided for right-handed twist, as coming from shear caused by interdigitating termini, is particular to the right-twisting structure which was generated to match the experimental data on ILQINS. It is established that multiple thermodynamically equivalent structures can exist for peptide fibrils of this type, with either large or small structural differences between them.[62,63] Other causes of twist might exist for right-twisting fibrils in which the termini do not take part in the amyloid structure as advanced for the α-synuclein case.[64]

CONCLUSIONS

We have identified the hexameric peptide sequence ILQINS that is ubiquitous in amyloid fibrils formed from HEWL. Experimental evidence showed that a helical ribbon conformation with a rarely found right-handedness is the preferred morphology for these systems. A combination of X-ray scattering and molecular dynamics simulations was used to obtain an atomistic structure of the fibrillar unit cell. The simulations show that this right-handed twist originates from intersheet stresses. The fibrils assembled with rapid kinetics (<90 s) as demonstrated by AFM, CD, and synchrotron SAXS/WAXS studies. At longer reaction times a fibril-crystal conversion was observed. The fundamental principles of amyloid assembly elucidated here can aid the rational design of future amyloid based biomaterials or biomimetic hybrids. Our results infer that right twist can be promoted by ensuring that assembly of fibrils along the peptide backbone axis (a) kinetically or energetically dominates that along the side-chain (b) axis. Our observations also provide a first conclusive explanation for the known phenomenon that right twist can be disrupted by mutations at the termini of the peptide strands. Control of the elastic stresses has long been used in the design and study of lipid membrane self-assembly, and this work represents an important step toward the same understanding and control in the case of amyloid aggregation of peptides.

ASSOCIATED CONTENT

Supporting Information

Materials and methods, amino acid sequence determination from MALDI-MS. Results of the sequence prediction algorithm, NMR, and MS characterization of synthetic ILQINS fragment. CD measurements, SAXS form factor used to fit flat crystalline structures at long incubation times, and additional AFM images. This material is available free of charge via the Internet at http://pubs.acs.org.

AUTHOR INFORMATION

Corresponding Author

raffaele.mezzenga@hest.ethz.ch

Author Contributions

The manuscript was written through contributions of all authors. All authors have given approval to the final version of the manuscript. C.L. and N.P.R. contributed equally to this work.

Notes

The authors declare no competing financial interest.

ACKNOWLEDGMENTS

We thank Dr. Serge Chesnov from the Functional Genomics Center in Zurich for the MALDI-MS experiments. N.P.R. would like to thank the Swiss National Science Foundation for a personal fellowship (PBSKP2_145829) and Dr. Nigel Kirby and Dr. Adrian Hawley for assistance at the SAXS/WAXS beamline at the Australian Synchrotron. R.M. wishes to thank Dr. Jozef Adamcik (ETH) for helpful discussions. The synchrotron-based research in this work was in part supported by the Science and Industry Endowment Fund (SEIF) Special Research Program - Synchrotron Science. All supercomputer resources were provided by the University of Luxembourg HPC facility. A.X. and A.Z. thank the financial support from the National Natural Science Foundation of China (no. 21034004).

REFERENCES

(1) Chiti, F.; Dobson, C. M. *Annu. Rev. Biochem.* **2006**, *75*, 333−366.
(2) Luheshi, L. M.; Crowther, D. C.; Dobson, C. M. *Curr. Opin. Chem. Biol.* **2008**, *12*, 25−31.
(3) Kayed, R.; Head, E.; Thompson, J. L.; McIntire, T. M.; Milton, S. C.; Cotman, C. W.; Glabe, C. G. *Science* **2003**, *300*, 486−489.
(4) Conway, K. A.; Lee, S. J.; Rochet, J. C.; Ding, T. T.; Williamson, R. E.; Lansbury, P. T. *Proc. Natl. Acad. Sci. U.S.A.* **2000**, *97*, 571−576.
(5) Winner, B.; Jappelli, R.; Maji, S. K.; Desplats, P. A.; Boyer, L.; Aigner, S.; Hetzer, C.; Loher, T.; Vilar, M.; Campionic, S.; Tzitzilonis, C.; Soragni, A.; Jessberger, S.; Mira, H.; Consiglio, A.; Pham, E.; Masliah, E.; Gage, F. H.; Riek, R. *Proc. Natl. Acad. Sci. U.S.A.* **2011**, *108*, 4194−4199.
(6) Reynolds, N. P.; Soragni, A.; Rabe, M.; Verdes, D.; Liverani, E.; Handschin, S.; Riek, R.; Seeger, S. *J. Am. Chem. Soc.* **2011**, *133*, 19366−19375.
(7) Bellotti, V.; Mangione, P.; Merlini, G. *J. Struct. Biol.* **2000**, *130*, 280−289.
(8) Brandner, S.; Isenmann, S.; Raeber, A.; Fischer, M.; Sailer, A.; Kobayashi, Y.; Marino, S.; Weissmann, C.; Aguzzi, A. *Nature* **1996**, *379*, 339−343.
(9) Fowler, D. M.; Koulov, A. V.; Alory-Jost, C.; Marks, M. S.; Balch, W. E.; Kelly, J. W. *PLoS Biol.* **2006**, *4*, 100−107.
(10) Maji, S. K.; Perrin, M. H.; Sawaya, M. R.; Jessberger, S.; Vadodaria, K.; Rissman, R. A.; Singru, P. S.; Nilsson, K. P. R.; Simon, R.; Schubert, D.; Eisenberg, D.; Rivier, J.; Sawchenko, P.; Vale, W.; Riek, R. *Science* **2009**, *325*, 328−332.
(11) Greenwald, J.; Riek, R. *Structure* **2010**, *18*, 1244−1260.

(12) Knowles, T. P. J.; Buehler, M. J. *Nat. Nanotechnol.* **2011**, *6*, 469−479.
(13) Adamcik, J.; Lara, C.; Usov, I.; Jeong, J. S.; Ruggeri, F. S.; Dietler, G.; Lashuel, H. A.; Hamley, I. W.; Mezzenga, R. *Nanoscale* **2012**, *4*, 4426−4429.
(14) Reynolds, N. P.; Styan, K. E.; Easton, C. D.; Li, Y.; Waddington, L.; Lara, C.; Forsythe, J. S.; Mezzenga, R.; Hartley, P. G.; Muir, B. W. *Biomacromolecules* **2013**, *14*, 2305−2316.
(15) Bongiovanni, M. N.; Scanlon, D. B.; Gras, S. L. *Biomaterials* **2011**, *32*, 6099−6110.
(16) Cherny, I.; Gazit, E. *Angew. Chem., Int. Ed.* **2008**, *47*, 4062−4069.
(17) Li, C.; Adamcik, J.; Mezzenga, R. *Nat. Nanotechnol.* **2012**, *7*, 421−427.
(18) Geddes, A. J.; Parker, K. D.; Atkins, E. D. T.; Beighton, E. *J. Mol. Biol.* **1968**, *32*, 343−344.
(19) Sunde, M.; Serpell, L. C.; Bartlam, M.; Fraser, P. E.; Pepys, M. B.; Blake, C. C. F. *J. Mol. Biol.* **1997**, *273*, 729−739.
(20) Guijarro, J. I.; Sunde, M.; Jones, J. A.; Campbell, I. D.; Dobson, C. M. *Proc. Natl. Acad. Sci. U.S.A.* **1998**, *95*, 4224−4228.
(21) Dobson, C. M. *Trends Biochem. Sci.* **1999**, *24*, 329−332.
(22) Cheng, P.-N.; Pham, J. D.; Nowick, J. S. *J. Am. Chem. Soc.* **2013**, *135*, 5477−5492.
(23) Sawaya, M. R.; Sambashivan, S.; Nelson, R.; Ivanova, M. I.; Sievers, S. A.; Apostol, M. I.; Thompson, M. J.; Balbirnie, M.; Wiltzius, J. J. W.; McFarlane, H. T.; Madsen, A. O.; Riekel, C.; Eisenberg, D. *Nature* **2007**, *447*, 453−457.
(24) Marshall, K. E.; Serpell, L. C. *Soft Matter* **2010**, *6*, 2110−2114.
(25) Wiltzius, J. J. W.; Landau, M.; Nelson, R.; Sawaya, M. R.; Apostol, M. I.; Goldschmidt, L.; Soriaga, A. B.; Cascio, D.; Rajashankar, K.; Eisenberg, D. *Nat. Struct. Mol. Biol.* **2009**, *16*, 973−U98.
(26) Liu, L.; Busuttil, K.; Zhang, S.; Yang, Y.; Wang, C.; Besenbacher, F.; Dong, M. *Phys. Chem. Chem. Phys.* **2011**, *13*, 17435−17444.
(27) Scanlon, S.; Aggeli, A. *Nano Today* **2008**, *3*, 22−30.
(28) Silva, G. A.; Czeisler, C.; Niece, K. L.; Beniash, E.; Harrington, D. A.; Kessler, J. A.; Stupp, S. I. *Science* **2004**, *303*, 1352−1355.
(29) Arnaudov, L. N.; de Vries, R. *Biophys. J.* **2005**, *88*, 515−526.
(30) Frare, E.; de Laureto, P. P.; Zurdo, J.; Dobson, C. M.; Fontana, A. *J. Mol. Biol.* **2004**, *340*, 1153−1165.
(31) Tartaglia, G. G.; Pawar, A. P.; Campioni, S.; Dobson, C. M.; Chiti, F.; Vendruscolo, M. *J. Mol. Biol.* **2008**, *380*, 425−436.
(32) Frare, E.; Mossuto, M. F.; de Laureto, P. P.; Dumoulin, M.; Dobson, C. M.; Fontana, A. *J. Mol. Biol.* **2006**, *361*, 551−561.
(33) Lara, C.; Adamcik, J.; Jordens, S.; Mezzenga, R. *Biomacromolecules* **2011**, *12*, 1868−1875.
(34) Krebs, M. R. H.; Wilkins, D. K.; Chung, E. W.; Pitkeathly, M. C.; Chamberlain, A. K.; Zurdo, J.; Robinson, C. V.; Dobson, C. M. *J. Mol. Biol.* **2000**, *300*, 541−549.
(35) Thompson, M. J.; Sievers, S. A.; Karanicolas, J.; Ivanova, M. I.; Baker, D.; Eisenberg, D. *Proc. Natl. Acad. Sci. U.S.A.* **2006**, *103*, 4074−4078.
(36) Lara, C.; Handschin, S.; Mezzenga, R. *Nanoscale* **2013**, *5*, 7197−7201.
(37) Cenker, C. C.; Bucak, S.; Olsson, U. *Soft Matter* **2011**, *7*, 4868−4875.
(38) Ribo, J. M.; Crusats, J.; Sagues, F.; Claret, J.; Rubires, R. *Science* **2001**, *292*, 2063−2066.
(39) Volpatti, L. R.; Vendruscolo, M.; Dobson, C. M.; Knowles, T. P. J. *ACS Nano* **2013**, *7*, 10443−10448.
(40) Harper, J. D.; Lieber, C. M.; Lansbury, P. T. *Chem. Biol.* **1997**, *4*, 951−959.
(41) Koga, T.; Matsuoka, M.; Higashi, N. *J. Am. Chem. Soc.* **2005**, *127*, 17596−17597.
(42) Rubin, N.; Perugia, E.; Goldschmidt, M.; Fridkin, M.; Addadi, L. *J. Am. Chem. Soc.* **2008**, *130*, 4602−4603.
(43) Kurouski, D.; Dukor, R. K.; Lu, X.; Nafie, L. A.; Lednev, I. K. *Biophys. J.* **2012**, *103*, 522−531.
(44) Usov, I.; Adamcik, J.; Mezzenga, R. *ACS Nano* **2013**, *7*, 10465−10474.
(45) Kurouski, D.; Dukor, R. K.; Lu, X. F.; Nafie, L. A.; Lednev, I. K. *Chem. Commun.* **2012**, *48*, 2837−2839.
(46) Chung, D. S.; Benedek, G. B.; Konikoff, F. M.; Donovan, J. M. *Proc. Natl. Acad. Sci. U.S.A.* **1993**, *90*, 11341−11345.
(47) Marshall, K. E.; Hicks, M. R.; Williams, T. L.; Hoffmann, S. V.; Rodger, A.; Dafforn, T. R.; Serpell, L. C. *Biophys. J.* **2010**, *98*, 330−338.
(48) Lewandowski, J. R.; van der Wel, P. C. A.; Rigney, M.; Grigorieff, N.; Griffin, R. G. *J. Am. Chem. Soc.* **2011**, *133*, 14686−14698.
(49) Adamcik, J.; Jung, J.-M.; Flakowski, J.; De Los Rios, P.; Dietler, G.; Mezzenga, R. *Nat. Nanotechnol.* **2010**, *5*, 423−428.
(50) Najbar, L. V.; Craik, D. J.; Wade, J. D.; Salvatore, D.; McLeish, M. J. *Biochemistry* **1997**, *36*, 11525−11533.
(51) Yang, J. J.; Pitkeathly, M.; Radford, S. E. *Biochemistry* **1994**, *33*, 7345−7353.
(52) Manning, M. C.; Illangasekare, M.; Woody, R. W. *Biophys. Chem.* **1988**, *31*, 77−86.
(53) Glatter, O. *Neutrons, X-rays and Light: Scattering Methods Applied to Soft Condensed Matter*, 1 st ed.; Elsevier: Amsterdam, The Netherlands, 2002, pp 73−103.
(54) Borsali, R.; Pecora, R. *Soft Matter Characterization*; Springer Science: New York, 2008, pp 57−68.
(55) Pronchik, J.; He, X.; Giurleo, J. T.; Talaga, D. S. *J. Am. Chem. Soc.* **2010**, *132*, 9797−9803.
(56) Rabe, M.; Soragni, A.; Reynolds, N. P.; Verdes, D.; Liverani, E.; Riek, R.; Seeger, S. *ACS Chem. Neurosci.* **2013**, *4*, 408−417.
(57) Gillam, J. E.; MacPhee, C. E. *J. Phys.: Condens. Matter* **2013**, *25*, 373101.
(58) Knowles, T. P. J.; Oppenheim, T. W.; Buell, A. K.; Chirgadze, D. Y.; Welland, M. E. *Nat. Nanotechnol.* **2010**, *5*, 204−207.
(59) Soininen, A. J.; Kasemi, E.; Schlueter, A. D.; Ikkala, O.; Ruokolainen, J.; Mezzenga, R. *J. Am. Chem. Soc.* **2010**, *132*, 10882−10890.
(60) Mezzenga, R.; Fischer, P. *Rep. Prog. Phys.* **2013**, *76*, 046601.
(61) Nelson, R.; Sawaya, M. R.; Balbirnie, M.; Madsen, A. O.; Riekel, C.; Grothe, R.; Eisenberg, D. *Nature* **2005**, *435*, 773−778.
(62) Berryman, J. T.; Radford, S. E.; Harris, S. A. *Biophys. J.* **2009**, *97*, 1−11.
(63) Berryman, J. T.; Radford, S. E.; Harris, S. A. *Biophys. J.* **2011**, *100*, 2234−2242.
(64) Hoyer, W.; Antony, T.; Cherny, D.; Heim, G.; Jovin, T. M.; Subramaniam, V. *J. Mol. Biol.* **2002**, *322*, 383−393.